www.rericjournal.ait.ac.th

Solar Driven LiBr-H_2O Absorption Chiller Simulation to Analyze Two Backup Options

Furugaan Ibrahim*, Surapong Chirarattananon*, ϕ, #, 1, Pattana Rakkwamsuk^, Pipat Chaiwiwatworakul*, ϕ, #, Surawut Chuangchote+, and Vu Duc Hien†

ARTICLE INFO

Article history:
Received 16 April 2021
Received in revised form
15 July 2021
Accepted 26 July 2021

Keywords:
Absorption chiller
ASRC-CIE sky model
Simulation
Solar cooling
Vapor compression chiller

ABSTRACT

Solar cooling technologies are becoming increasingly popular. Technological innovation and mass production driven due to its use of renewable energy has led to a significant reduction in the initial cost of investment. However, due to the sporadic nature of solar energy coupled with other technical and economical limitations, it is difficult to solely depend on a solar cooling system. In this study, a solar powered absorption chiller system was mathematically modelled and simulated. Objective of this study was to compare the performance of an absorption chiller system using two backup modes; LPG fired auxiliary heating mode and using an electrically driven vapor compression chiller. Inclined solar collectors were generating the solar power for the system. Solar irradiance on the inclined plan of the solar collector were calculated using ASRC-CIE sky model. Sky model and the absorption chiller with auxiliary heater was validated by dissecting the system into major components and comparing the results with practically logged data. Both configurations were able to meet the cooling requirements. Annual simulations of the two systems showed that both systems could operate with a collector area to cooling power ratio of 2 m^2/kW_{th}.

1. INTRODUCTION

Thailand is located at a tropical region where for the northern part of Thailand, weather could be rainy, warm, or cloudy depending on the time of the year, but usually hot and humid for the southern part of Thailand. Air-conditioning is used in all regions of Thailand. A study conducted in Thailand reports that air-conditioning, in residential and commercial buildings contribute to 40-60% of electrical energy consumed [1].

Solar techniques are becoming popular. Its environmental friendliness and its use of renewable energy to bring the desired outcome is one of the driving factors for this. Studies show that the increasing popularity and technological innovations results in a decreasing trend of cost for solar cooling systems [2], [3]. Additionally, with the increase of environmental concerns and consumption of fossil fuels, solar industry is on a rapidly increasing trend [4]. Solar PV is becoming more popular, and globally installed capacity of solar thermal technologies reported were significant [5], [6]. Cost of these systems is a huge factor driving the popularity of these systems. While smalls systems in residential scale have a significantly higher cost compared to split systems available in the market, large scale systems show a significant reduction in cost making it financially more viable [7], [8]. Amongst the available solar thermal technologies, at a large scale, cost of absorption chillers is lower than other thermally activated systems [9], [10]. Therefore, it is anticipated that soon, absorption chillers would be competing with conventional cooling systems.

The sporadic nature of solar energy makes it necessary to install a backup option with solar powered absorption chiller. Commonly used backup modes include heating system at the heat generator side or an electrically driven vapor compression chiller [11]. Backup options could be configured in series or parallel. For an auxiliary heater in a series arrangement, flow always goes through the auxiliary heater boosting the hot water temperature. In a parallel configuration, depending on the hot water temperature, flow would bypass the auxiliary heater. Since primary energy savings are low for single-effect absorption chillers, utilizing auxiliary heaters have been reported to be inefficient, and has been only recommended for double or triple effect absorption chillers [11]. Furthermore,

*The Joint Graduate School of Energy and Environment, King Mongkut's University of Technology Thonburi, Bangkok, Thailand.

+Science and Technology Postgraduate Education and Research Development Office, Ministry of Education, Thailand.

#Center of Excellence on Energy Technology and Environment, Ministry of Education Thailand.

^School of Energy, Environment and Materials, King Mongkut's University of Technology Thonburi, Bangkok, Thailand.

+Department of Tool and Materials Engineering, Faculty of Engineering, King Mongkut's University of Technology Thonburi, Bangkok, Thailand.

†Sustainable Energy Transition program, Asian Institute of Technology, Pathum Thani, Thailand.

1Corresponding author:
Email: surapong@jgsee.kmutt.ac.th.

gas-fired backup systems are appropriate only if the auxiliary heat required is less [12].

Similarly, vapor compression chillers can be arranged in a parallel or series configuration. In a parallel configuration, either vapor compression chiller or absorption chiller operates to meet the demand. However, in series configuration, both systems work together to meet the demand. A system without a backup will either be undersized; which runs at rated conditions without being able to meet the cooling requirement during some critical conditions of the year or, will be oversized; which will operate below rated conditions most of the time. Furthermore, fluctuating hot water temperatures in an absorption chiller system without backup also causes phase instability during the operation [13].

In this study, a single effect absorption chiller with two backup modes was considered. In both cases, the connection was parallel. In the first case, LPG fired burner was used as an auxiliary heater to boost the hot water temperature whenever it was below 75°C. In the second case, an electrically driven vapor compression chiller was used to meet the demand whenever hot water temperature was below 75°C.

Since the solar collectors, or the heating system is one of the major contributions to the total cost, objective of this study was to investigate how much solar collector area could be compromised with the addition of an electric chiller to this system [14], [15]. Also, to do an evaluation on the performance of absorption chiller with two backup modes. Due to the limitations (economically and technologically) in completely relying on renewable technologies, the rationale behind such a hybrid configuration was to ease the transitional phase of shifting to renewable energy technologies. In this study, a full system simulation model was used to illustrate the allowable reduction in collector area. Three locations of Thailand would be discussed throughout the paper. Therefore, for ease of understanding, these locations have been listed in Table 1 along with the part of work that was carried out at that location.

Table 1. Locations and work carried out in that location.

Location	Part covered
Naresuan University, Phitsanulok.	Absorption Chiller setup used in this paper was setup here. Experiment data for the validation of absorption chiller system was collected from this university.
Asian Institute of Technology, Khlong Luang, Pathumthani	2013 Weather data used for the annual simulations were collected from station at this university.
Bangkunthian Campus, King Mongkut University of Technology Thonburi, Bangkok.	Weather data collected to validate the sky model was collected from the station at this university.

2. SYSTEM

Absorption chiller used in this study was modelled according to a system installed in Naresuan University, Phitsanulok, Thailand (16°N latitude and 100°E longitude). Various Performance studies and economical studies have been conducted and published for this system [14] - [17]. Simulation model was developed and, absorption chiller part was calibrated and validated using practical data obtained from the site.

2.1 Configuration

The system in Naresuan University was equipped with a 35 kW LiBr-H_2O absorption chiller (Yazaki WFC SC-10) powered by 72 m^2 evacuated tube solar collector and an LPG fired Rinnai 32e backup heating system. Solar collectors were installed on roofs that were inclined at a 20° slope towards south-east. Cooling water was provided by a 175kW cooling tower. Installed hot water storage and chilled water storage tanks were 0.5m^3 and 0.2m^3 by volume respectively. In this system, solar collector generates thermal energy (hot water) storing it in the hot water tank. LPG heater acting as an auxiliary source, boosts the temperature of the hot water when the solar energy was in- sufficient for the absorption chiller to operate. Water vapor in the LiBr-H_2O solution gets boiled within the absorption chiller by this hot water as it is pumped into it. Condenser cools down this water vapor, which then is passed to the evaporator. Cooling effect is brought about when this water gets evaporated again at low pressure. The process has been further elaborated in the next section.

2.2 Mathematical Modelling

Figure 1 illustrates the configuration and the mathematical model used in this study. Note that for the case of simulation, additional back-up mode (parallel electric chiller) was introduced to the practical model as mentioned earlier.

Mathematical model discussed in this paper uses meteorological data as an input. Cooling load of the space was evaluated using 'BESim'. BESim was developed and used during the development of Thailand building energy code [18] and was also used in thermal performance studies [17], [18]. In this program, dynamic heat transfer was calculated employing energy balance with meteorological data as an input. Accuracy of heat transfers were ensured by using numerically calculated view factors, taking into consideration the long and short-wave radiations. BESim was coded using C++, and the calculated cooling load from BESim was fed into the absorption chiller model (coded in MATLAB) together with the meteorological data. Cooling load evaluated from BESim, irradiance on the inclined plane, and weather data was then used as an input to the absorption chiller system model. Subsequent temperatures at the end of every time step were evaluated by simple energy balance. This section will

elaborate on how the system was mathematically modeled.

As seen in the Figure 1, two backup modes were simulated in this study. In the first mode (which would be referred to as "case 1"), LPG fired auxiliary heater was used. In the second backup mode (which would be referred to as "case 2"), electrical chiller was utilized as a backup. For both modes, temperature of the of the hot water tank determines the purpose of the backup. For case 1, when the hot water temperature was below 75°C, auxiliary heater would be on and water would pass through auxiliary heater before being supplied to the absorption chiller. For case 2, when the hot water temperature was below 75 °C, electric chiller would be turned on, and the absorption chiller would go to standby mode. At this time electrical chiller would be exchanging heat with chilled water tank, while solar hot water heating system would be charging the hot water tank. When the hot water tank gets sufficiently charged, electrical chiller would switch to standby mode and vice versa.

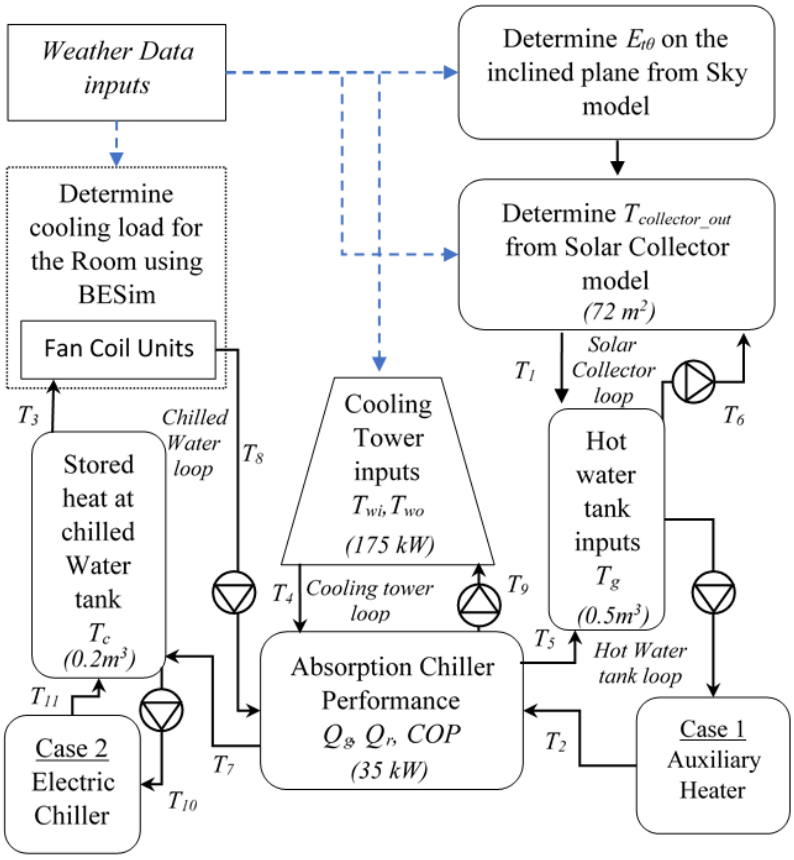

Fig. 1. System Configuration and mathematical model.

2.2.1 Sky model

Sky model was used to determine the total irradiance on the inclined solar collector plane. Using measured meteorological data at the horizontal plane, irradiance was evaluated with ASRC-CIE sky model. The model was originally for sky illuminance, however authors claimed that it could be used for sky irradiance with certain approximations [19]. ASRC-CIE sky model is a linear summation of four other sky models; clear sky model (*cl*), turbid clear sky model (*tcl*), intermediate sky model (*in*), and overcast sky model (*oc*) as given in Equation 1. The coefficients b_{xx} is determined by the Perez clearness index and brightness index, and *E* refers to the irradiance.

$$E_{ed} = b_{cl}E_{cl} + b_{tcl}E_{tcl} + b_{in}E_{in} + b_{oc}E_{oc} \quad (1)$$

Using the sky model, the irradiance of 145 standard sky points was determined. These points were assumed to be very small, and ground reflected irradiance was neglected. For each data point, the diffuse sky irradiance on the inclined plane and the total irradiance on the inclined plan ($E_{t\theta}$) were later evaluated using simple vector geometry assuming that the earth was flat. In the simulation, a 13.6° inclined surface facing south was used. Uniform sky model compared to irradiance obtained from ASRC-CIE sky model also showed a good resemblance [20].

2.2.2 Absorption system model

a) Solar collector model and thermal storage system model

Solar collector model would give the heat generated from the solar collector for given conditions. Evacuated tube collectors were used as a primary thermal power source for the single effect absorption chiller. Efficiency curve of the collectors used in this study was given by Equation 2 [21], and the useful heat gain was evaluated using this equation. For the collector used in this study,

the manufacturer gives $\in_0$, a_1, and a_2 as 0.717, 1.52, and 0.0085, respectively. Using $T_{Collector-out}$, temperature of the hot water tank (T_g) was evaluated using energy balance at every time step. Hot water, and chilled water storage tanks were assumed to be well mixed and modelled by doing a simple energy balance at every time step.

$$\in = \in_0 - a_1 \frac{(T_{Collector-out} - T_{amb})}{E_{t\theta}} - a_2 \frac{(T_{Collector-out} - T_{amb})^2}{E_{t\theta}} \quad (2)$$

where;

$\in$: Efficiency of the collector (%)
$\in_0$ Zero loss collector efficiency (%)
a_1 : Heat transfer coefficient *($W.m^{-2}.K^{-1}$)*
a_2 : Heat transfer coefficient *($W.m^{-2}.K^{-2}$)*
$T_{Collector-out}$: Temperature water out from the collector *(K)*
T_{amb} : Ambient temperature *(K)*
$E_{t\theta}$: Total irradiance on the inclined collector plane *($W.m^{-2}$)*

b) Room model for cooling load

A 20 m by 20 m room as illustrated in Figure 2, was modelled and the cooling load required from 8:00 AM to 5:00 PM for the whole year was calculated using BESim. The building has window to wall ratios of 0.28, 0.38, 0.24, and 0.38 to facades facing west, north, east, and south directions, respectively. Figure 3 demonstrates a scatter plot of the cooling loads calculated from BESim, and the average cooling load between 8:00AM and 5:00PM.

Fig. 2. Room model.

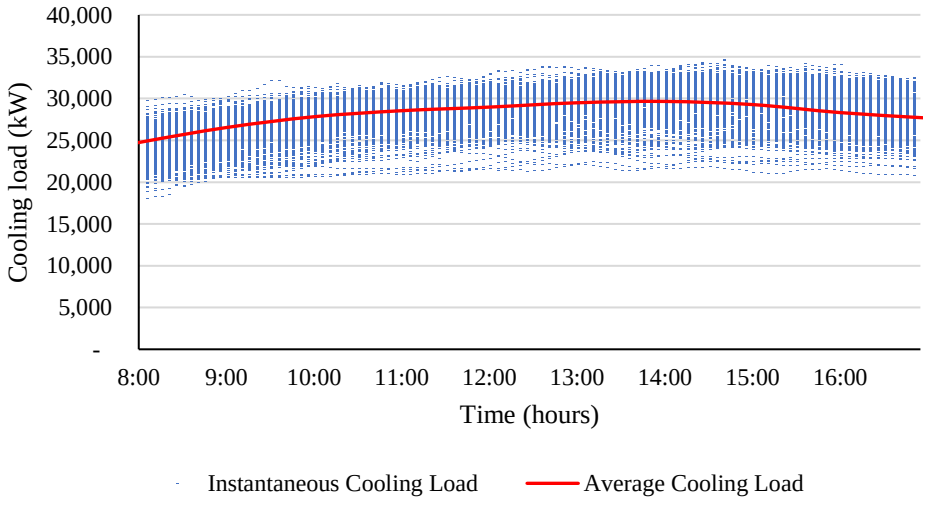

Fig. 3. Calculated cooling load from BESim.

The correlation coefficient of the calculated cooling loads to global irradiance and ambient temperature was 0.792 and 0.936, respectively. Therefore, fluctuations of cooling load due to these weather factors were well accounted, for the purpose of this paper. The purpose of using this model, rather than fixing the cooling load was because the cooling output of the absorption chiller also depends on these weather conditions. Hence, the comparison would be more acceptable when the cooling load of the building also varies with these weather conditions.

c) Absorption chiller and electrical chiller model

Yazaki WFC SC-10 absorption chiller was modelled using a second order polynomial curve. Polynomial

regression models adopting performance curves provided by the manufactures have been reported to be highly accurate [22]. A second order polynomial equation for three variables could be expressed as in Equation 3. Both refrigeration heat output (Q_r) and coefficient of performance (COP) was expressed using the same equation as a function (f) of hot water temperature into the chiller (T_g), cooling water into the chiller (T_{wi}), and chilled water temperature out of the chiller (T_c). Using the performance curves of the system provided by the manufacturer (as in Figure 4), two sets of coefficients a_{ij} , b_{ij} , and c_{ij} were calculated using least squares curve fitting method for both Q_r and COP

$$
\begin{aligned}
&f(T_c, T_{wi}, T_g) = \\
&(c_{11} + c_{12}T_c + c_{13}{T_c}^2) + (c_{21} + c_{22}T_c + c_{23}{T_c}^2)T_{wi} \\
&+(c_{31} + c_{32}T_c + c_{33}{T_c}^2){T_{wi}}^2 + \\
&[(b_{11} + b_{12}T_c + b_{13}{T_c}^2) + (b_{21} + b_{22}T_c + b_{23}{T_c}^2)T_{wi} \\
&+(b_{31} + b_{32}T_c + b_{33}{T_c}^2){T_{wi}}^2]T_g + \\
&[(a_{11} + a_{12}T_c + a_{13}{T_c}^2) + (a_{21} + a_{22}T_c + a_{23}{T_c}^2)T_{wi} \\
&+(a_{31} + a_{32}T_c + a_{33}{T_c}^2){T_{wi}}^2]{T_g}^2
\end{aligned}
\tag{3}
$$

$$
Q_g = \frac{Q_r}{COP} \tag{4}
$$

$$
Q_{CL} = Q_r + Q_g \tag{5}
$$

The curves on Figure 4 shows how the performance of absorption chiller (Q_r and COP) varies with T_c and, at constant T_{wi} (T_{wi} = 29.5℃) . Similar sets of performance curves were given by the manufacturer for different sets of T_{wi} ranging from 24℃ to 32℃. Once Q_r and COP were identified, hot water generated (Q_g) and cooling tower input (Q_{CL}) were calculated using Equations 4 and 5.

$$
\begin{aligned}
&f(T_c, T_{amb}) = \\
&c_1 + c_2T_c + c_3T_{amb} + c_4{T_c}^2 + c_5T_cT_{amb} \\
&+c_6{T_{amb}}^2 + c_7{T_c}^3 + c_8{T_c}^2T_{amb} + c_9T_c{T_{amb}}^2
\end{aligned}
\tag{6}
$$

$$
P_{Elct} = \frac{Q_{re}}{COP_e} \tag{7}
$$

Major assumptions in the model include no heat exchange between the ambient and the components and throttle valves had zero enthalpy loss. As for the backups, auxiliary heater for case 1 was modeled as a heat exchanger with hot air and water tube. For case 2, a DAIKIN (EUWA*8kBZW1) electrical chiller was modelled using a third order polynomial curve with both electrical refrigeration heat output (Q_{re}) and coefficient of performance (COP_e) expressed as a function (f) of ambient temperature (T_{amb}) and chilled water temperature out of the chiller (T_c) as given in Equation 6. Employing the performance curves provided by the manufacturer (as in Figure 5), two sets of coefficients (c_i) were evaluated by using least square curve fitting method for both Q_{re} and COP_e . Once Q_{re} and COP_e were known, electrical power (P_{Elct}) was calculated using Equation 7.

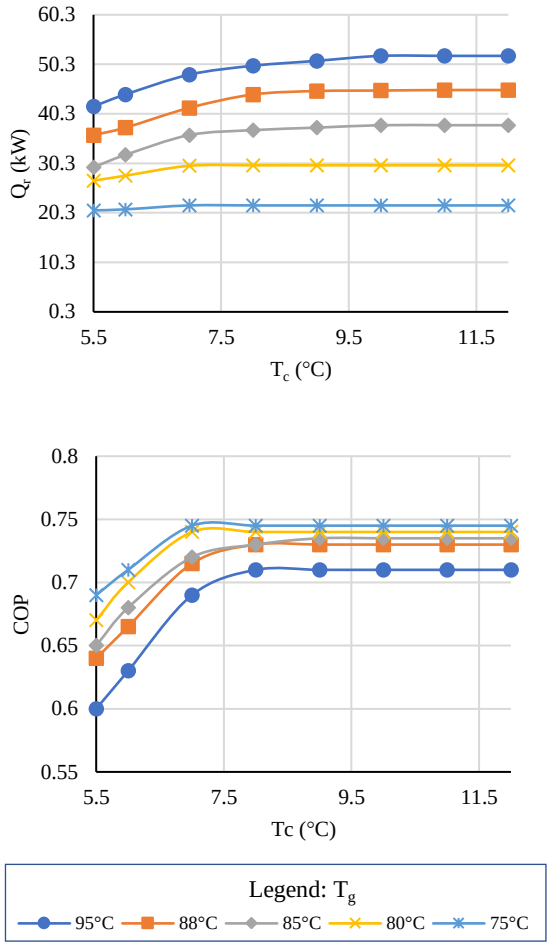

Fig. 4. Qr and COP of the absorption chiller at T_{wi} = 29.5℃.

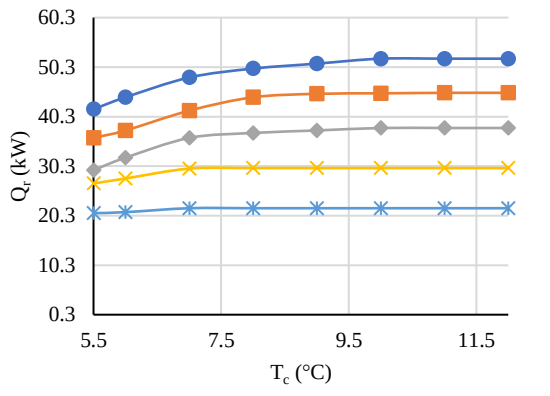

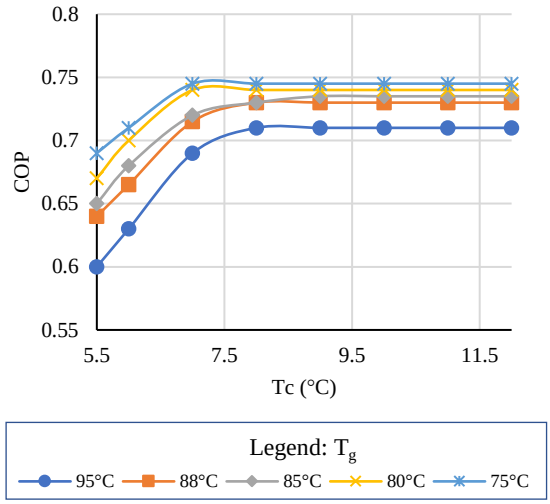

Fig. 5. Q_{re} **and** P_{Elct} **of electrical chiller and different chilled water temperatures.**

d) Dehumidifying coil model

Fan coil model was adapted from a model by Chirarattananon [23] based on cooling coil calculations in HVAC systems and Equipment in ASHRAE 2005 [24]. This dehumidifying coil model was to evaluate the final condition of the room, and the condition of chilled water returning to the chiller after cooling the space. Initially, the model estimates the heat transfer in the coil based on the input conditions of air, the refrigerant, and the physical parameters of the cooling coil. Then after estimating the dividing point of the wet and dry section of the coil, calculations were done to find the heat transfer at each section. Initial estimate would be then adjusted based on the summation of the wet and dry areas until the total area of the coil and the summed areas were within an acceptable range.

e) Cooling Tower model

Cooling tower is the component in the absorption chiller providing cooling water which enables the removal of heat from the absorption chiller. A counter flow cooling tower was modeled based on the number of transfer units (NTU) correlation derived and reported by Chirarattananon [25]. This was based on correlations derived earlier as given in Equation 8 [26]. In this model, an ideal case of heat transfer was assumed such that the enthalpy of air leaving the cooling tower was the enthalpy of saturated air at the temperature of water flowing in. Based on the selected size and the designed operating conditions of the cooling tower provided by the manufacturer, the values of '*a*' and '*n*' used were 0.9325 and 0.4887, respectively.

$$NTU = a\left(\frac{m_c}{m_a}\right)^n \tag{8}$$

2.2.3 *Validation of models*

Due to the complexity of the system coupled with the availability of data from different locations and different time, a part-by-part approach was applied to validate the system. The whole system was allotted into six water loops: solar collector loop (*ScLoop*), cooling tower loop (*CtLoop*), hot water tank loop (*HwtLoop*), chilled water tank loop (*CwtLoop*), auxiliary heating loop (*AuxLoop*), and absorption chiller loop (*AbsLoop*). Sky model was validated separately using measured irradiance data. For the vapor compression electrical chiller introduced in case 2, since no chiller was available for the experiment, the model was validated by comparing the results with the data provided by the manufacturer.

In the loop validation approach, each component's output was compared with the experimental data. For example, in the case of the collector, an imaginary control volume was assumed around the collector (as shown in Figure 6). The inputs to the collector model were the collector parameters, inlet water temperature, and input weather data based on actual data recorded. Outlet water temperature calculated from the model (X) was then compared with the outlet water temperature of the recorded data (Y) for the same time step. Similarly, cooling tower, hot water tank, chilled water tank, auxiliary heater, and absorption chiller was validated by assuming a control volume around the component. Same inputs as the recorded data were fed into the model, and calculated outputs were compared with the recorded experimental outputs.

$$R^2 = \left(\left(\frac{1}{N}\right)\sum \frac{\left(X_i - \overline{X}\right)\left(Y_i - \overline{Y}\right)}{\left(\sigma_X \times \sigma_Y\right)}\right)^2 \tag{9}$$

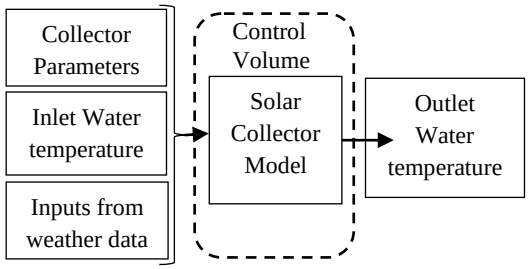

Fig. 6. Collector loop validation.

Figure 7 shows the temperatures evaluated from the mathematical model compared to those logged from the practical operations. Figure also shows the coefficient of determination (R^2) calculated for all the major components of the system. R^2 was calculated using Equation 9, where X and Y were the outputs from model and outputs recorded at the station, respectively. The results conclude that the models were in good agreement with the actual setup. A lower coefficient of determination for the absorption chiller could be because the chiller was not mechanically at the same condition as when the chiller was while the manufactures data were plotted. Also, experimentally, it is difficult to achieve steady state condition since ambient conditions and load conditions were varying. However, Table 2 shows the coefficient of determination calculated for the polynomial curve fitting based on the manufacturers data. Looking at both Table 2 and the values listed in Figure 7, it can be reasonably

to concluded that absorption chiller was in good agreement with the model. As for the values given for electrical chiller in Table 2, since there were no practical data for this chiller, only validation conducted was how well the polynomial curve fitting represents the manufacturers data. Higher coefficient of determination for the electrical chiller also validated that the model was in good agreement with the actual system. Propagated error from the measurements and calculations were also calculated using the law of propagation and found to be within 8.62%, 10.50%, 0.50%, 0.1%, 5.16%, and 9.12%, for temperature, *RH*, pressure, flow, *COP*, and Q_r, respectively.

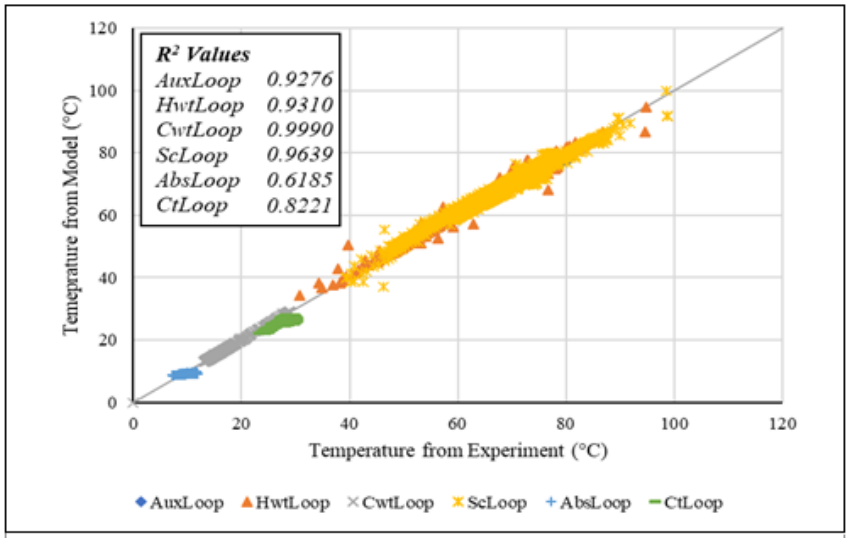

Fig. 7. Temperatures obtained from mathematical model compared to practical values.

Fig. 8. Pyranometer setup at to measure weather data.

Table 2. Coefficient of determination calculated for polynomial curve fitting.

Loop	R^2
Absorption chiller Q_r	0.9928
Absorption chiller *COP*	0.8939
Electrical Chiller Q_r	0.9999
Electrical Chiller *COP*	0.9964

Since the solar collectors were at an inclined position, evaluating the irradiance on the inclined plane was also important for a full system model. Figure 8 shows the Pyranometer setup at Bangkunthain Campus of King Mongkut's University of Technology Thonburi, Bangkok, Thailand. Initially, the pyronometer was placed horizontally to calibrate with the stationed pyronometer, and then it was inclined to 13.6° facing south. The comparison of irradiance evaluated using the ASRC-CIE sky model on the measured horizontal plane and on the measured inclined plane were illustrated in Figure 9. As per results, the model compared to

measured horizontal irradiance was with a coefficient of determination of 0.9992. Likewise, the model compared to measured irradiance on the inclined plane was with a coefficient of determination of 0.9930, with a slight deviation at higher irradiance values. Both horizontal and inclined values have been presented because, values on the horizontal plane were the values that were originally achieved from the ASRC-CIE sky model.

Upon the completion of the validation of the individual parts, a full simulation of the absorption chiller was due. The system in Naresuan University was not in operational condition in 2017 at the time of the site visit, hence experimental data needed for the validation could not be obtained during then. Next available option during the time frame was to use logged data from earlier operations. Note that for a full system simulation, meteorological data (from the weather station at Naresuan University) and data from absorption chiller was needed. Since data logging were done by two individual data loggers, a time frame when both meteorological station and absorption chiller were operational had to be selected. Table 3 set out one such time frame between 11:57 AM to 12:03 PM on 11th December 2007 for which experimental data were compared to simulation data. However, even for this case, simulation was initiated from the solar collector (excluding the sky model), and irradiance recorded on the inclined plane were used. A full system simulation initiating from the sky model could not be conducted due to missing necessary meteorological data coinciding with the chiller operation time.

T_1, T_2, T_3, T_4, and T_7 in Table 3 are temperatures of hot water generated from solar collector, temperature of hot water supplied to the absorption chiller, temperature of chilled water supplied to the fan coil, temperature of cooling water supplied to the chiller by the cooling tower, and chilled water produce by the chiller respectively (refer to Figure 1). Table 3 demonstrates that simulated temperatures were similar to the values obtained from the experiment.

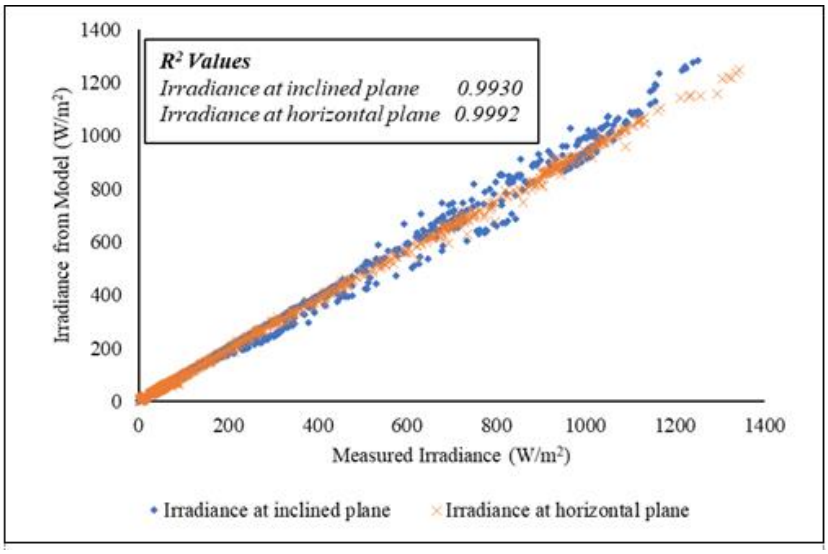

Fig. 9. Irradiance from sky model compared at horizontal and inclined plane.

Table 3. Experimental data (Exp) and simulation data (Sim) at selected points.

Weather conditions		T_1 (°C)		T_2 (°C)		T_4 (°C)		T_3 (°C)		T_7 (°C)	
T_{amb} (°C)	$E_{t\theta}$ (W/m^2)	Exp	Sim	Exp	Sim	Exp	Sim	Exp	Sim	Exp	Sim
31.31	741.26	89.40	*88.66*	85.23	*85.81*	28.70	*27.28*	10.19	*10.18*	9.70	*9.50*
31.45	735.84	88.84	*87.92*	84.49	*85.23*	28.85	*27.24*	10.26	*10.17*	10.72	*9.38*
31.53	716.24	88.39	*87.14*	84.07	*84.50*	28.96	*27.47*	9.85	*9.97*	9.43	*9.38*
31.58	716.69	87.72	*86.75*	83.72	*84.08*	29.04	*27.19*	10.00	*9.88*	10.14	*9.33*
31.65	744.69	87.23	*86.57*	83.11	*83.73*	29.07	*27.23*	9.90	*9.88*	10.15	*9.29*
31.14	755.75	86.79	*86.18*	82.75	*83.11*	28.98	*26.86*	9.60	*9.67*	9.18	*9.30*
31.31	747.05	86.32	*85.71*	82.39	*82.76*	28.86	*26.84*	9.82	*9.67*	10.22	*9.25*

2.3 Simulation of the System

With the validated models, next part of the study was to conduct annual simulations. For the annual simulations, 2013 weather data collected at a 5-minute basis from station located at Asian Institute of Technology in Bangkok Thailand was utilized. For simplification, all the volume flow rates were kept constant, except the chilled water flowrate at FCU which depended on the cooling load. During the simulation, T_2 and T_6 were equal to the temperature of the water in the hot water

storage tank at i^{th} hour. T_1 was evaluated using Equation 2 while Q_r and *COP* calculated using the performance curves with T_2, T_4 and T_7 as inputs. T_9 and T_5 were evaluated using Equation 4 and 5, respectively. Resultant temperature of water in the tank was then calculated by doing an energy balance of the energy in the tank and the heat supplied to and from the tank to give the T_2 and T_6 at $i+1$ hour. T_4 for $i+1$ hour was computed from the cooling tower model.

Table 4 shows the simulation data for a selected day (10th February) and time for Case 1. Initially, Auxiliary heater was on since T_2<75°C. As T_2>75°C at 10:10, auxiliary heater was switched off, and the absorption chiller started to operate with only solar collector heating system. Table 5 illustrates for the same day and time, how the system operated under Case 2. While T_2<75°C, absorption chiller was on standby mode, and electrical chiller was supplying the chilled water to the tank. Simultaneously, the solar hot water heating system was running to charge the hot water tank. When T_2>75°C, electrical chiller goes to standby mode, and absorption chiller starts to operate.

Table 4. Simulation results for 10th February (Case 1).

Time (Hrs)	T_{amb} (°C)	$E_{t\theta}$ (Wm^{-2})	T_2 (°C)	T_7 (°C)	Q_r (kW)	Q_g (kW)	Q_{AUX} (kW)
09:50	29.04	228.37	71.38	8.52	6.57	7.83	6.20
09:55	28.84	193.38	71.50	8.52	6.53	7.76	6.08
10:00	29.05	280.51	72.19	8.51	6.42	7.64	6.04
10:05	29.76	538.33	74.51	8.52	6.61	7.96	5.81
10:10	30.45	545.79	76.80	8.57	7.28	9.01	5.06
10:15	30.76	579.86	79.23	8.60	7.61	9.53	-
10:20	31.40	550.95	81.42	8.62	7.87	10.10	-
10:25	30.98	511.97	83.28	8.63	8.00	10.39	-

Table 5. Simulation results for 10th February (Case 2).

Time (Hrs)	T_{amb} (°C)	$E_{t\theta}$ (Wm^{-2})	T_2 (°C)	T_7 (°C)	Q_r (kW)	Q_g (kW)	$Q_{r,e}$ (kW)
09:50	29.04	228.37	73.58	7.69	-	-	11.75
09:55	28.84	193.38	74.06	7.65	-	-	11.78
10:00	29.05	280.51	75.10	7.60	-	-	11.75
10:05	29.76	538.33	77.53	8.30	3.77	4.65	-
10:10	30.45	545.79	79.79	8.52	6.58	8.32	-
10:15	30.76	579.86	82.16	8.59	7.43	9.57	-
10:20	31.40	550.95	84.27	8.62	7.82	10.27	-
10:25	30.98	511.97	86.06	8.63	7.99	10.60	-

3. RESULTS AND DISCUSSION

During the annual simulations, the effect on Q_r, Q_g, *AUX* heat, and Q_{re} would be analyzed in three scenarios. The scenarios considered were by varying the size of the chilled water tank storage (scenario V-CS), by varying hot water tank storage (scenario V-HS), and by varying collector area (scenario V-COLL). These effects were illustrated in Figures 10 to 12. Annual thermal energies were plotted on the vertical axis. Horizontal axis shows the corresponding collector areas for the curve with varying collector area, and top horizontal axis shows the corresponding tank volumes for the curves with varying thermal storage. “V-CW”, “V-COLL”, and “V-HW” in the plot legends refer to varying chilled water tank size, varying collector area, and varying hot water tank size, respectively. Table 6 shows the description of the cases and scenarios considered in the simulations.

In the simulations, collector area was kept constant at 72 m^2, chilled water and hot water storage tanks were kept constant at 1m^3 except when it was the variant in that particular scenario. For example, Q_r generated annually under Case 1 (Figure 10) shows that 26,667 kWh was generated with a hot water tank of 1.25 m^3 (from V-HW curve). This means that for this case and scenario collector area was 72 m^2 and the chilled water storage tank was 1 m^3. Similarly, 24,407 kWh was generated with a collector area of 60 m^2 (from V-COLL curve). This means both thermal storages were 1 m^3.

Table 6. Description of the cases and scenarios.

Case	Abbreviation	Description
Case	1	System with auxiliary heater as backup
	2	System with vapor compression chiller as backup
Scenario	V-CS	Varying chilled water storage tank size
	V-HW	Varying hot water storage tank size
	V-COLL	Varying collector area

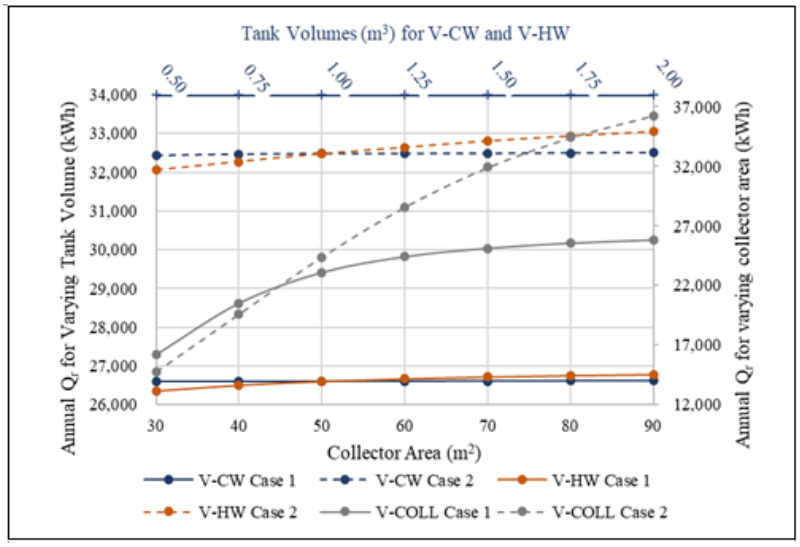

Fig. 10. Effect on Q_r generated annually for Case 1 and Case 2 by varying thermal storage and collector area.

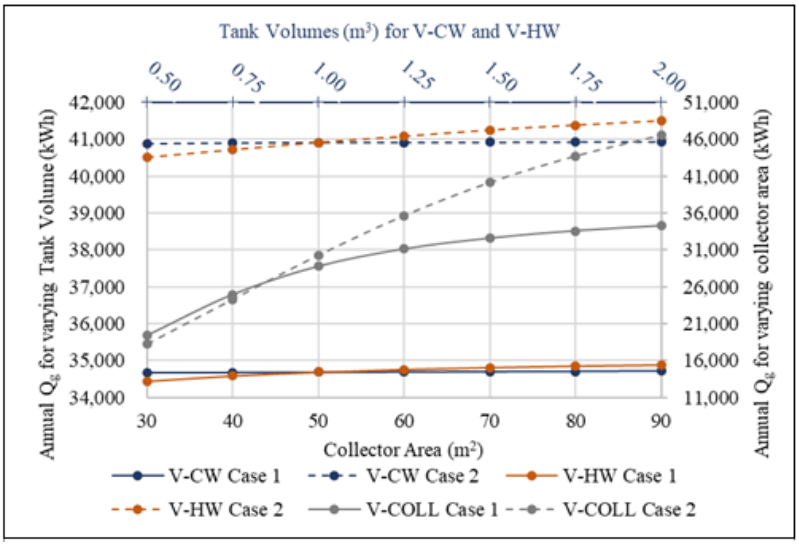

Fig. 11. Effect on Q_g total generated annually for Option 1 and Case 2 by varying thermal storage and collector area.

Analysis of the plots indicates that, for Case 1 and Case 2, the effect of changing chilled water storage tank was small on Q_r, Q_g, *AUX* heat (for Case 1), and Q_{re} (for Case 2) generated annually. Table 7 presents a variation of 2.5% between the minimum and maximum volume of chilled water storage simulated. As for increasing the hot water storage tank, Q_r and Q_g increases with the increase in tank size, while *AUX* heat (for Case 1) and Q_{re} (for Case 2) decreases with the decrease in tank size. Table also shows the variation of Q_{re} to be below 6.5% between the minimum and maximum hot water storage tank volume for case 2, while *AUX* heat generated for case 2 varied by 43.8%. This is because the increase in volume needed additional heat to be generated to maintain at a particular temperature.

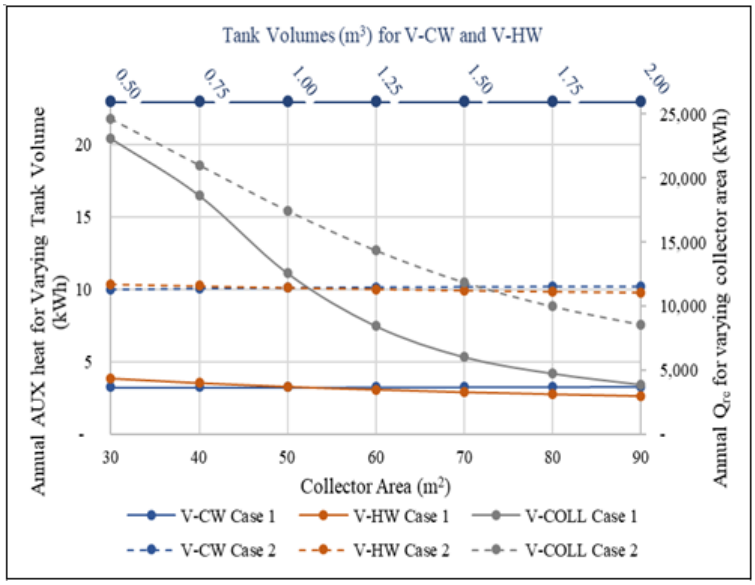

Fig. 12. Effect of auxiliary heat generated and Qr generated from electric chiller by varying thermal storage and collector area.

Table 7. Percentage variation between the minimum and maximum of each.

Scenario	Case 1			Case 2		
	Q_r	Q_g	*AUX*	Q_r	Q_g	Q_{re}
V-CW	0.140868	0.122836	0.338027	0.225175	0.172585	2.456346
V-COLL	37.13709	43.18469	-494.715	59.36651	60.73591	-187.522
V-HW	1.584791	1.285524	-43.7597	3.038091	2.377906	-6.50818

Lastly, for the collector area, Q_r and Q_g initially increases when the collector area was increased. Then the slope becomes constant and later decreased with the increase of collector area. Table 7 shows the variation to be as high as 494.7% for auxiliary heat generated. In the case of *AUX* heat (for Case 1) and Q_{re} (for Case 2), initially both decreases with the increase in collector area. Then the slope decreases, and upon further increase in collector area, it showed that *AUX* heat (for Case 1) and Q_{re} (for Case2) tends to increase slightly. This would be explained by using average temperature of hot water tank and chilled water tank at different collector areas (as shown in Figure 13). When collector area was small, the average temperature at which the hot water tank maintained was lower. Hence, it was passing through the auxiliary heater more often, which raised the temperature of the water to a significant amount. This resulted in a higher Q_r at times, while maintaining average chilled water tank temperature low. Hence with a lower chilled water tank temperature, annually generated Q_r was lower because of the decrease in delta T (delta T of the tank, based on which chiller would supply chilled water to tank, and delta T from the load side, where lower chilled water temperature would result in a lower delta T to meet the space load). When the collector area increases slightly, and when the temperature of the hot water tank was just above 75°C, this low-grade hot water goes to the chiller (without the need of the auxiliary heater). Due to this, Q_r generated was lower at times, and average chilled water temperature of the tank was higher. Because of this, at times when the hot water temperature was higher, chiller generated higher Q_r due to the higher delta T. Upon further increase in collector area, with the availability of higher-grade heat, system was able to maintain the chilled water tank at a lower temperature, eventually decreasing the Q_r generated annually.

Studies report 4.23m^2/kW_{th} to be an ideal collector area to absorption chiller capacity [27], while another reports 8m^2/kW_{th} as the optimum collector area [28]. One study also reports that the optimum ratio varies from 0.2 – 5 m^2/kW_{th} [29]. While climate and configuration have a huge impact on this ratio, [30] reports that 4m^2/kW_{th} shows a significant increase in performance on a solar cooling autonomous system. Further stating that the effect decreases when the ratio increased beyond 4.5m^2/kW_{th}. Figures 11 to 12 increase effect of increase in collector area (slope) decreases as the collector area increases. Furthermore, increase in collector area would raise the investment cost of the system. Taking all the above into consideration, 2 m^2/kW_{th} was found to be an optimum ratio the configuration discussed in this study. Further analysis on an optimum ratio could be done by doing economic analysis of the system. It should also be noted that a similar ratio is used in the system at Naresuan University.

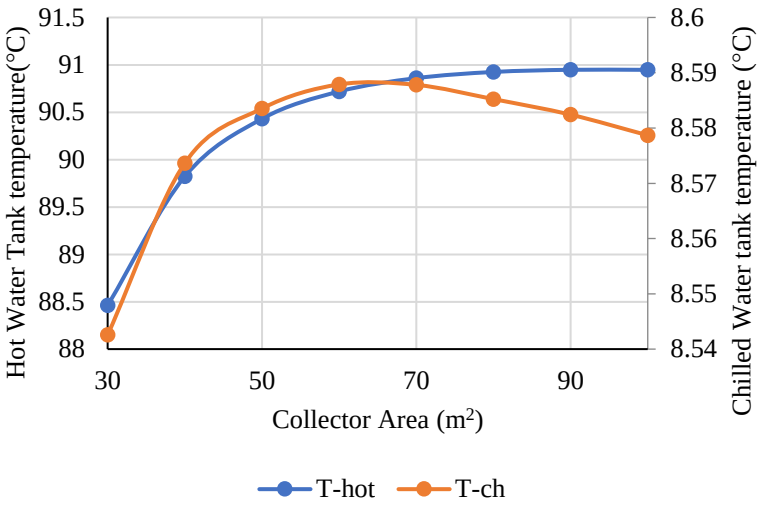

Fig. 13. Average temperature of hot water tank and chilled water tank.

Both backup modes discussed in this paper demonstrated a similar performance. Even though the LPG fired system was applicable for this case, this may not be so viable for a large-scale system. One main advantage of an electrical chiller is, that with the use of electrical chiller, the system could be operated in a hybrid mode instead of a backup mode. That is by connecting the electrical chiller and absorption chiller in a series mode rather than in parallel. In this case, electrical chiller, and absorption chiller both would be working on chilled water tank giving combined chilled effect of both absorption chiller and electrical chiller. This could be easily achieved by using some valves to manipulate the connections.

3. CONCLUSION

- Using ASCR-CIE sky model and other geometrical relationships, irradiance on the inclined plane could be calculated with a coefficient of determination of 0.99.
- Absorption chiller model used in this paper evaluates the output of the system which was in good agreement with the actual system.
- For the simulated configuration in this study, varying chilled water storage tank does not have much effect on the performance of the system. However, increasing the volume of hot water storage tank increased the performance of the system.
- Effect of collector area output was limited by the hot water storage tank volume. Within a certain range, the collector area was extremely sensitive to the output, while the effect becomes less sensitive as the collector area increased beyond a certain amount. Upon further increase in collector area, annual output showed a slight decrease in the hot water output. For this configuration, an optimum collector area was found to be around 70 m^2 (2 m^2/kW_{th}) in terms of performance.

ACKNOWLEDGEMENT

The authors would like to express their gratitude to The Joint Graduate School of Energy and Environment (JGSEE), King Mongkut's University of Technology Thonburi and the Center of Excellence on Energy Technology and Environment (CEE), PERDO, Ministry of Higher Education, Science, Research and Innovation for the financial support provided to perform this study.

REFERENCES

[1] Chirarattananon S. and V.D. Hien. 2011. Thermal performance and cost effectiveness of massive walls under thai climate. *Energy & Buildings* 43(7): 1655-1662.

[2] Otanicar T., Taylor R.A., and Phelan P.E., 2012. Prospects for solar cooling – An economic and environmental assessment. *Solar Energy* 86(5): 1287-1299.

[3] Zeyghami M., Goswami D.Y., and Stefanakos E., 2015. A review of solar thermo-mechanical refrigeration and cooling methods. *Renewable and Sustainable Energy Reviews* 51: 1428–1445.

[4] Kannan N. and D. Vakeesan. 2016. Solar energy for future world: - A review. *Renewable and Sustainable Energy Reviews* 62: 1092-1105.

[5] REN21 Renewables Now. 2019. Renewables 2019 Global Status Report.

[6] Herold K.E., Radermacher R., and Klein S.A., 2016. *Absorption chillers and heat pumps*. 2nd ed. USA: CRC Press.

[7] Kohlenbach P. and M. Dennis. 2010. Solar cooling in Australia: The future of air-conditioning? *Ecolibrium Aust Inst Refrig. Air Cond. Heat* 12: 32-38.

[8] Beccali M., Ceullar M., Finocchiaro P., Guarino F., Longo S., and Nocke B., 2012. Life cycle assessment performance comparison of small solar thermal cooling systems with conventional plants assisted with photovoltaics. *Energy Procedia* 30: 893-903.

[9] Zhai X.Q., Qu M., Li Y., and Wang R.Z., 2011. A review for research and new design options of solar absorption cooling systems. *Renewable Sustainable Energy Reviews* 15: 4416-4423.

[10] Kim D.S. and Infante Ferreira C., 2008. Solar refrigeration options – A state-of-the-art review. *International Journal of Refrigeration* 31(1): 3-15.

[11] Shirazi A., Taylor R.A., Morrison G.L., and White S.D., 2018. Solar-powered absorption chillers: A comprehensive and critical review. *Energy Conversion Management* 171: 59-81.

[12] Calise F., Palombo A. and Vanoli L., 2010. Maximization of primary energy savings of solar heating and cooling systems by transient simulations and computer design of experiments. *Applied Energy* 87(2): 524-540.

[13] Marc O., Sinama F., Praene J.P., Lucas F., and Castaing-Lasvignottes J., 2015. Dynamic modeling and experimental validation elements of a 30 kW LiBr/H2O single effect absorption chiller for solar application. *Applied Thermal Engineering* 90: 980–993.

[14] Yongprayun S., Ketjoy N., Rakwichian W., and Maneewan S., 2007. Techno-economic analysis of a LiBr-H2O Solar Absorption Cooling System in Thailand. *International Journal of Renewable Energy* 2(2): 1–10.

[15] Pongtornkulpanich A., Thepa S., Amornkitbamrung M., and Butcher C., 2008. Experience with fully operational solar-driven 10-ton LiBr/H2O single-effect absorption cooling system in Thailand. *Renewable Energy* 33(5): 943–949.

[16] Ketjoy N., Rawipa Y., and Mansiri K., 2013. Performance evaluation of 35 kW LiBr H2O solar absorption cooling system in Thailand. *Energy Procedia* 34: 198-210.

[17] Laodee P., Suriwong T. and Somkun S., 2016. Performance of non-CFC refrigerator driven by chilled water from 35 kW LiBr / H 2 O solar absorption cooling system. *International Journal of Renewable Energy* 11(2): 35-40.

[18] Chirarattananon S., Rakwamsuk P., Hien V.D., and Taweekun J., 2004. Development of a Building Energy Code for New Buildings in Thailand. In *Sustainable Energy and Environment Conference*. Hua Hin, Thailand, 1-3 December.

[19] Kobav M. and G. Bizjak. 2013. Sky Luminance Models. In Beckers B, ed. *Solar Energy at Urban Scale*. John Wiley & Sons, pp 37–56.

[20] Ibrahim F., 2013. A comparative study of small solar absorption and PV-driven chiller. Master Thesis, King Mongkut's University of Technology Thonburi, Bangkok, Thailand (unpublished).

[21] Föste S., Giovannetti F., Ehrmann N., and Rockendorf G., 2014. Performance and reliability of a high efficiency flat plate collector – Final results on prototypes. *Energy Procedia* 48: 48–57.

[22] Labus J., Bruno J.C., and Coronas A., 2013. Performance analysis of small capacity absorption chillers by using different modeling methods. *Applied Thermal Engineering* 58(1-2): 305–313.

[23] Chirarattananon S., 2005. Holistic approach to calculation of energy use in buildings. In *Building for Energy Efficiency*. Building Energy Management Project, pp 319-383.

[24] ASHRAE., 2005. Air-cooling and dehumidifying Coils. In *HVAC Systems and Equipment* ASHRAE.

[25] Chirarattananon S., 2005. Cooling Tower. In *Building for Energy Efficiency*. Building Energy Management Project, pp 366-372.

[26] Braun J.E., Clain S.A. and Mitchell J.W., 1989. Effectiveness Modes for Cooling Towers and Cooling Coils. *ASHRAE Transactions*. 95: 164-174.

[27] Ali A.H.H., Noeres P., and Pollerberg C., 2008. Performance assessment of an integrated free cooling and solar powered single-effect lithium bromide-water absorption chiller. *Solar Energy* 82(11): 1021-1030.

[28] García Cascales, J.R., Vera García F., Cano Izquierdo J.M., Delgado Marín J.P., and Martínez Sánchez R., 2011. Modelling an absorption system assisted by solar energy. *Applied Thermal Energy* 31(1): 112–118.

[29] Eicker U. and D. Pietruschka. 2009. Design and performance of solar powered absorption cooling systems in office buildings. *Energy and Buildings* 41(1): 81–91.

[30] Keeratianant S., Chirarattananon S., Nathakaranakule A., and Rakkwamsuk P., 2019. Cost-effectiveness of solar cooling for office and hypermarket. *Applied Science and Engineering Progress*: 1–13.